# Magnetic properties of $Fe_3Si$/GaAs(001) hybrid structures

K. Lenz,* E. Kosubek, K. Baberschke, and H. Wende
*Institut für Experimentalphysik, Freie Universität Berlin, Arnimallee 14, D-14195 Berlin, Germany*

J. Herfort, H.-P. Schönherr, and K. H. Ploog
*Paul-Drude-Institut für Festkörperelektronik, Hausvogteiplatz 5-7, D-10117 Berlin, Germany*
(Received 22 March 2005; published 11 October 2005)

The magnetic properties of two epitaxial $Fe_3Si$/GaAs(001) hybrid structures are studied using ferromagnetic resonance. The results from the angular dependence of the excited uniform mode enable a precise determination of the magnetic anisotropy fields in this ferromagnet/semiconductor hybrid structure. The samples differ in their Si content (one stoichiometric sample with 25.5% and one Fe-rich with 16.5% Si). Moderate effective magnetizations of $4\pi M_{\text{eff}}=10.1$ kG and 13.5 kG, respectively, were found. In addition, depending on the Si content in the Heusler-like alloy, a small but pronounced uniaxial in-plane anisotropy field of $2K_{2\|}/M=-6$ to $-32$ Oe with the easy axis rotated by 45° with respect to the easy axis of the larger fourfold anisotropy exists.

DOI: 10.1103/PhysRevB.72.144411 PACS number(s): 76.50.+g, 75.30.Gw, 75.50.Bb, 75.70.Ak

## I. INTRODUCTION

Ferromagnetic metals grown epitaxially on semiconducting substrates is today's basic need for the development of magnetoelectronic devices.[1] Apart from the extensively studied ferromagnetic elements Fe[2–8] or Co[9] grown epitaxially on GaAs(001) substrate, the Heusler-like alloy $Fe_3Si$ is rather unnoticed,[10–12] although this system has many advantages: (i) the cubic $D0_3$ crystal structure of $Fe_3Si$ is almost lattice matched to the GaAs(001) substrate, providing a highly epitaxial growth and high interfacial perfection,[13] (ii) the high Curie temperature of 840 K,[14] and (iii) the thermal stability of the ferromagnet/semiconductor (FM/SC) interface up to 700 K is also favorable in terms of applicability to magnetoelectronics.[12] Structural characterization by double-crystal x-ray diffraction[10,13] measurements, spin injection studies,[15] and initial magnetic characterization by superconducting quantum interference device (SQUID) magnetometry[10] has been done. The hysteresis loops taken by the SQUID show that the easy axis of magnetization is in the film plane along the ⟨100⟩ directions with a small, temperature independent coercive field of $H_C \leqslant 1$ Oe. Moreover, a difference in the magnetization loops was observed for the [110] and $[\bar{1}10]$ directions for low Si content similar to pure Fe films. For the stoichiometric sample (with 25.5% Si content), the loops were almost identical. To clarify this, we determined the magnetic anisotropy constants using ferromagnetic resonance (FMR) for two samples.

## II. FMR EXPERIMENTS

The $Fe_3Si$ films were grown by molecular beam epitaxy. The GaAs(001) templates were prepared in a separate III-V growth chamber using standard growth conditions. The $(2\times1)$ As-rich reconstructed GaAs(001) substrate was then transferred into an As-free chamber through UHV, where the $Fe_3Si$ films were prepared by co-deposition from high-temperature effusion cells onto the substrate at 200 °C.[13] The growth of the samples was monitored *in situ* by reflection high-energy electron diffraction (RHEED) technique. The FMR experiments were performed with microwave frequencies of 1.1, 4.1, and 9.2 GHz at ambient temperature for two samples *A* and *B*, to cross-check the anisotropy parameters and to determine the FMR dispersion relation. Sample *A* contains 25.5% Si (stoichiometric), and *B* 16.5% Si (Fe-rich). The samples are 39 nm and 33 nm thick, respectively. The Si content of the films was determined from the position of the $Fe_3Si$ layer peak using double crystal x-ray diffraction.[13] The FMR was detected angular dependent, i.e., with respect to the orientation of the externally applied magnetic field $\vec{H}$. Figure 1 contains a sketch of the coordinate system used: $\varphi$ and $\varphi_H$ are the azimuthal, and $\theta$ and $\theta_H$ are the polar angles of the magnetization $\vec{M}$ and the external field $\vec{H}$, respectively, and $\varphi_u$ is the rotation of the easy axis of

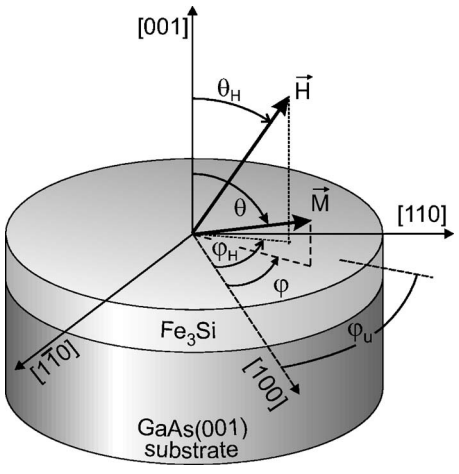


FIG. 1. Sketch of the coordinate system used. $\varphi$ and $\varphi_H$ are the azimuthal, and $\theta$ and $\theta_H$ are the polar angles of the magnetization $\vec{M}$ and the external field $\vec{H}$, respectively. $\varphi_u$ is the rotation of the easy axis of the uniaxial in-plane anisotropy with respect to the easy axis of the fourfold anisotropy.

 

the uniaxial in-plane anisotropy with respect to the [100] direction, i.e., the easy axis of the fourfold anisotropy. Figure 2 shows three resonance spectra (absorption lines) of sample *A*. The first line taken with external field oriented parallel to the sample's plane ($\theta_H$=90°,$\varphi_H$=45°) and the second and third with nearly perpendicular direction. The resonance field shifts from 1 kOe up to 12.4 kOe due to a uniaxial (twofold) out-of-plane anisotropy. Note, since the FMR spectra are free of noise and the resonance linewidth are very narrow, we can precisely determine the resonance field $H_{\mathrm{res}(\theta,\varphi)}$ with an uncertainty less than 1%.

From this angular dependent measurement, i.e., by rotating the sample either within the sample plane (azimuthal angular dependence) or in the vertical plane spanned by the [001] and [110] axis (polar angular dependence), the anisotropy fields are obtained from the resonance field position $H_{\mathrm{res}}$ by a fit applying the Smit and Beljers[16] formalism,

$$\left(\frac{\omega}{\gamma}\right)^2 - \frac{(F_{\theta\theta}F_{\varphi\varphi} - F_{\theta\varphi}^2)}{M^2 \sin^2\theta} = 0, \tag{1}$$

with the free energy density $F$ of a single film,

$$\begin{aligned} F = &- MH[\sin\theta \sin\theta_H \cos(\varphi - \varphi_H) + \cos\theta \cos\theta_H] \\ &- (2\pi M^2 - K_{2\perp})\sin^2\theta + K_{2\parallel} \sin^2\theta \cos^2(\varphi - \varphi_u) \\ &- \frac{1}{2}K_{4\perp} \cos^4\theta - \frac{1}{8}K_{4\parallel}(3 + \cos 4\varphi)\sin^4\theta. \end{aligned} \tag{2}$$

In Eq. (1) $F_{ij}$ is the second partial derivative of $F$ with respect to $i$ and $j$, $K_{2\parallel}$ is the uniaxial in-plane and $K_{2\perp}$ the uniaxial out-of-plane anisotropy constant, and $K_{4\parallel}$ and $K_{4\perp}$ are the fourfold in—and out-of-plane anisotropy constants, respectively. The resulting resonance equation for polar rotation of the external field (under the assumption $\varphi = \varphi_H = \varphi_u$ =45°) is

$$\begin{aligned} \left(\frac{\omega}{\gamma}\right)^2 = &\left[ H_{\mathrm{res}} \cos(\theta - \theta_H) + \left( -4\pi M_{\mathrm{eff}} + \frac{2K_{2\parallel}}{M} + \frac{K_{4\perp}}{M} - \frac{K_{4\parallel}}{2M} \right) \right. \\ &\left. \times \cos 2\theta + \left( \frac{K_{4\perp}}{M} + \frac{K_{4\parallel}}{2M} \right) \cos 4\theta \right] \\ &\times \left[ H_{\mathrm{res}} \cos(\theta - \theta_H) + \left( -4\pi M_{\mathrm{eff}} + \frac{2K_{2\parallel}}{M} + \frac{K_{4\parallel}}{M} \right) \right. \\ &\left. \times \cos^2\theta + \left( \frac{2K_{4\perp}}{M} + \frac{K_{4\parallel}}{M} \right) \cos^4\theta - \frac{2K_{2\parallel}}{M} - \frac{2K_{4\parallel}}{M} \right], \end{aligned} \tag{3}$$

whereas for azimuthal rotation ($\theta = \theta_H$=90°) follows

$$\begin{aligned} \left(\frac{\omega}{\gamma}\right)^2 = &\left[ H_{\mathrm{res}} \cos(\varphi - \varphi_H) + 4\pi M_{\mathrm{eff}} \right. \\ &\left. - \frac{2K_{2\parallel}}{M} \cos^2(\varphi - \varphi_u) + \frac{K_{4\parallel}}{2M}(3 + \cos 4\varphi) \right] \\ &\times \left[ H_{\mathrm{res}} \cos(\varphi - \varphi_H) - \frac{2K_{2\parallel}}{M} \cos 2(\varphi - \varphi_u) \right. \\ &\left. + \frac{2K_{4\parallel}}{M} \cos 4\varphi \right], \end{aligned} \tag{4}$$

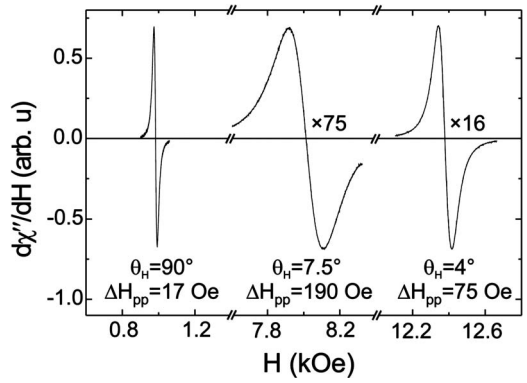


FIG. 2. FMR spectra of the stoichiometric sample *A*, taken at 9 GHz for three different polar orientations of the external magnetic field with $\varphi_H$=45°.

where $4\pi M_{\mathrm{eff}} = 4\pi M - 2K_{2\perp}/M$ is the effective magnetization. These resonance equations have to be evaluated at the equilibrium position of $\vec{M}$ under the applied external field determined by the minimum of $F$ by using the conditions $\partial F/\partial\theta = 0$ and $\partial F/\partial\varphi = 0$.

From Eqs. (2)–(4) and the spectra in Fig. 2 we see that a full angular dependent (polar and azimuthal) measurement of the FMR resonance enables us to determine unambiguously the various symmetry components of the anisotropy fields in second and fourth orders.[17] We would like to point out that, although at first glance this seems to be a fit with several fit parameters, the system is completely overdetermined, as we will show in the following section. If in addition such a complete set of experiments is performed at different microwave frequencies, we will be able to plot the FMR resonance positions as $f(H_{\mathrm{res}})$, the so-called resonance dispersion relation. We also would like to point out that the FMR does not measure in a direct way the magnetic anisotropy energies (MAE) as given in Eq. (2) but measures anisotropy fields as indicated in Eqs. (3) and (4), namely, dipolar fields $4\pi M$ or intrinsic anisotropy fields $K_i/M$. That in turn means that for the determination of the uniaxial and cubic anisotropy contributions $K_2$ and $K_4$, the knowledge of the saturation magnetization $M$ is necessary. For elementary ferromagnets like Fe, Co, or Ni this is simple. For compounds like $Fe_3Si$, it is more complicated. We will come back to this point in the next section.

## III. RESULTS AND DISCUSSION

The dispersion relation, i.e., the dependence of the resonance frequency on the external field, is shown in Fig. 3 for samples *A* and *B*. The lines are fits with Eq. (4) for the appropriate values of $\theta_H$ and $\varphi_H$, except for the dotted line of sample *A*, which shows a fit by Eq. (3) for the data taken in the [001] direction. For sample *B* the resonance line in the hard direction could not be detected due to field limitations. In the [110] and [1$\bar{1}$0] direction below 3 GHz for sample *A*

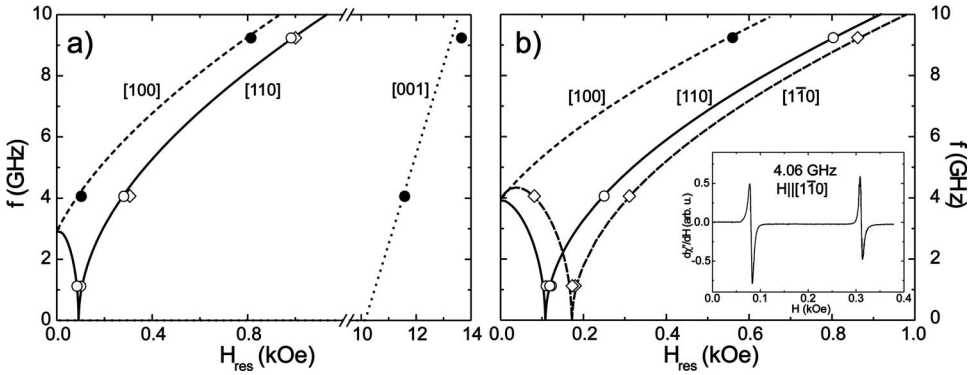


FIG. 3. Frequency dependence of the resonance lines position (dispersion relation) for (a) the stoichiometric sample *A* and (b) for the Fe-rich sample *B*. The dotted line is a fit with Eq. (3) and solid and dashed lines are fitted with Eq. (4). The inset in (b) shows the spectra for the $[\bar{1}10]$ measured at 4 GHz showing the unsaturated (lower field line) and saturated mode (higher field line).

and below 4.4 GHz for sample *B*, two resonance modes can be observed corresponding to two branches. The right branch (higher field line) represents the uniform (saturated) resonance mode, when magnetization $\vec{M}$ and external field $\vec{H}$ are aligned parallel. Thus, Eqs. (3) and (4) can be simplified using $\theta=\theta_H$ and $\varphi=\varphi_H$. On the left branch $\vec{M}$ and $\vec{H}$ are not aligned parallel anymore (unsaturated state); therefore, the equilibrium direction of $\vec{M}$ has to be calculated numerically. For sample *A* the fit for the $[1\bar{1}0]$ direction has been omitted for clarity, since it is almost identical to the [110] direction as one can see from the overlapping data points. For sample *B* the two directions are well distinguishable.

Figures 4(a) and 4(b) show the polar and azimuthal angular dependence of the resonance field for the stoichiometric sample *A* measured at 9 GHz. Figures 4(c) and 4(d) belong to sample *B*. The solid lines are the fits according to Eq. (3) for Figs. 4(a) and 4(c) and Eq. (4) for Figs. 4(b) and 4(d). From Figs. 4(a) and 4(c) it is clear that the hard axis lies in the [001] direction. A strong field is needed to tilt the magnetization against the uniaxial perpendicular anisotropy field to the sample's normal. Panels (b) and (d) in Fig. 4 show at first glance a fourfold (90°) symmetry with the easy axes being the in-plane ⟨100⟩ directions, whereas the in-plane ⟨110⟩ directions are intermediate ones. For sample *A* the effective magnetization is $4\pi M_{\mathrm{eff}}=4\pi M-2K_{2\perp}/M=10.1$ kG. A perpendicular fourfold anisotropy field of $2K_{4\perp}/M=-40$ Oe was also observed. Taking a closer look to Fig. 4(b) a small difference in the resonance field position of both maxima (along the $[1\bar{1}0]$ and [110]) is visible, slightly breaking the symmetry into a twofold symmetry due to a small uniaxial in-plane anisotropy field of $2K_{2\parallel}/M=-6$ Oe, favoring the [110] direction which modulates the larger fourfold anisotropy field of $2K_{4\parallel}/M=94$ Oe. This corresponds to the small nonequivalence seen in the SQUID hysteresis measurements of Ref. 10 (Figs. 5 and 6). Note that measurements over more than the simple periodicity are therefore essential. In contrast, the second sample shown in Figs. 4(c) and 4(d) has obviously larger anisotropy values, mainly due to the higher Fe content. The peak in the polar dependence [Fig. 4(c)] is much narrower, indicating an increased $4\pi M_{\mathrm{eff}}$. Also $2K_{4\perp}/M$ has increased from a negative value to zero. Nevertheless, the major difference compared to sample *A* is visible from the azimuthal angular dependence in Fig. 4(d). The "amplitude" has increased, denoting a larger $2K_{4\parallel}/M$, but the difference between the resonance position in the $[1\bar{1}0]$ and

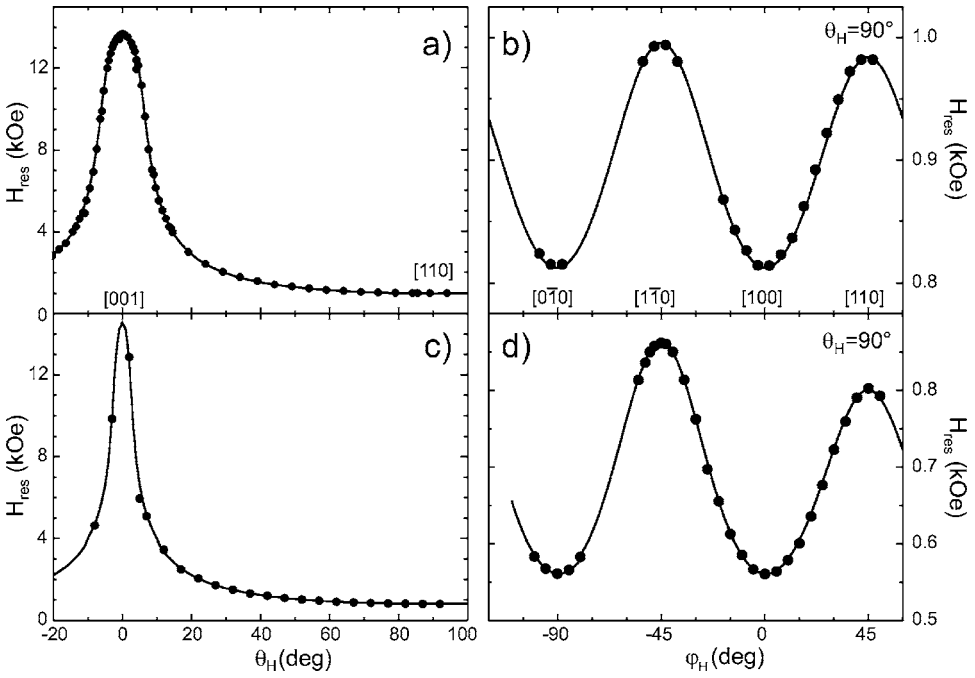


FIG. 4. (a) Polar and (b) azimuthal angular dependence of the resonance field measured at 9 GHz and ambient temperature, for the stoichiometric sample; (c) and (d) for the Fe-rich sample, respectively. The solid lines are fits according to Eqs. (3) and (4). The crystallographic directions are given in square brackets.

TABLE I. Anisotropy constants and effective fields of the 39- and 33-nm-thick samples *A* and *B* in comparison to values of a 21-nm-thick $Fe_3Si$/GaAs(001) sample (Ref. 11) and a 93-Å Fe/GaAs(001) sample (Ref. 18). The $Fe_3Si$ bulk value is $K_{4\|}=0.54\times10^5$ erg/cm$^3$ (Ref. 19). Error bars are due to 10% uncertainty in $M_S$; therefore, no expedient error bar can be given for $K_{2\perp}$.

| | Sample *A* 25.5% Si | Sample *B* 16% Si | $Fe_3Si$/GaAs(001) Ref. 11 | Fe/GaAs(001) Ref. 18 |
|---|---|---|---|---|
| $4\pi M-2K_{2\perp}/M$ (kG) | 10.10(2) | 13.50(2) | — | 20.8 |
| $K_{2\perp}$ ($10^5$ erg/cm$^3$) | −0.7 | −1.6 | — | — |
| $K_{2\|}$ ($10^5$ erg/cm$^3$) | −0.02(1) | −0.17(2) | −0.0046(9) | −0.4 |
| $K_{4\perp}$ ($10^5$ erg/cm$^3$) | −0.16(3) | 0 | — | — |
| $K_{4\|}$ ($10^5$ erg/cm$^3$) | 0.37(3) | 0.74(5) | 0.31(6) | 3.2 |

[110] directions has increased dramatically. The corresponding uniaxial in-plane anisotropy field $2K_{2\|}/M$ still favoring the [110] has increased by more than a factor of 5, whereas the effective magnetization $4\pi M_{\text{eff}}$ has increased by only 33% and $K_{4\|}$ by 50%.

In Table I the anisotropy parameters obtained from fitting are collected. To derive the anisotropy constants from the measured anisotropy fields we used a saturation magnetization of $M_S=790$ emu/cm$^3$ for sample *A* and $M_S=1050$ emu/cm$^3$ for sample *B* determined by SQUID measurements. Note that the error in $M_S$ is about 10% due to uncertainty in the sample volume. The anisotropy values are compared to results for a 21-nm-thick $Fe_3Si$/GaAs(001) film determined by Ionescu *et al.*[11] using the magneto-optic Kerr effect and a 93-Å-thick Fe/GaAs(001) film from Madami *et al.*[18] investigated by Brillouin light scattering. Comparing samples *A* and *B*, one can see that the anisotropy constants of sample *B* are by a factor of 2 to 8 larger than for *A*. Especially the uniaxial in-plane anisotropy $K_{2\|}$ has increased stronger than the other anisotropy contributions, while the Fe content was increased only by 12%. It is clear that with a Fe concentration higher than stoichiometric, the Fe atoms occupy Si sites. Moreover, from detailed structural investigations, it follows that in Fe-rich $Fe_3Si$/GaAs(001) a mixing of the Fe and Si sites occurs, i.e., Si occupies also regular Fe sites.[20] Thus the anisotropy is increased by the disorder effect which causes additional spin-orbit interaction. In the limit of high Fe content, the sample behaves like Fe/GaAs(001), where a large uniaxial in-plane anisotropy is well known.[18,21–24]

$K_{4\|}$ of the stoichiometric sample *A* agrees well with the findings of Ionescu *et al.*[11] Nevertheless, both are slightly smaller than the $Fe_3Si$ bulk value of $K_{4\|}=0.54\times10^5$ erg/cm$^3$.[19] The uniaxial in-plane anisotropy determined in Ref. 11 is about five times smaller than for sample *A*. This might be due to the different sample preparation, since a different substrate reconstruction and a higher growth temperature were used by Ionescu *et al.*[11] Compared to pure Fe films on GaAs(001) substrate, the values found in this work for $Fe_3Si$ are still 10 times smaller. However, the tendency of increasing MAE toward a pure Fe film is obvious, whereas a difference due to a different preparation of the GaAs interface (As-rich vs Ga-rich termination) can be ruled out.[21,22] In Fe/GaAs(001) the uniaxial in-plane anisotropy originates from the interface,[22–24] i.e., from an anisotropic Fe-Ga or Fe-As bonding structure where the dangling bonds of the topmost substrate layer have only a twofold symmetry. For Fe-rich $Fe_3Si$/GaAs(001) this should in principle be the same effect. In the stoichiometric sample the highly ordered structure of Si atoms alters the interface such that the twofold symmetry is suppressed and therefore $K_{2\|}$ is reduced. Here, a thickness dependent study of the MAE of $Fe_3Si$/GaAs(001) to separate the interface and volume contribution such as for Fe/GaAs(001)[6,22] would be clarifying. Moreover, strain effects may also play an important role, as the tetragonal distortion of the films is enlarged for increasing Fe content.

## IV. CONCLUSIONS

The present polar and azimuthal angular dependent FMR measurements determine very precisely the various components of the internal anisotropy fields: in- and out-of-plane contributions as well as twofold and fourfold components. Basically, the $Fe_3Si$ film is of cubic symmetry, but it appears that, depending on the Fe content, an uniaxial in-plane component also appears. From Table I we see that the Fe-rich film compared to the stoichiometric film shows increasing absolute contributions. For both samples *A* and *B* we find that the MAEs are smaller by a factor of approximately 10 than for a pure Fe film on GaAs. For technical application this reduction may be acceptable, still having the advantage of an ideal thermal and chemical stability of the $Fe_3Si$ interface compared to the metallic Fe films. Moreover, the possibility to select the strength of the uniaxial in-plane anisotropy by tuning the Fe concentration to the needs makes $Fe_3Si$/GaAs(001) an promising candidate for future magnetoelectronic devices.

## ACKNOWLEDGMENTS

This work was supported by the DFG (Sfb290 TP A2) and partly by BMBF (13N8255).

*Corresponding author. Email address: babgroup@physik.fu-berlin.de

[1] G. A. Prinz, Phys. Today **48** (4), 58 (1995).
[2] G. A. Prinz and J. J. Krebs, Appl. Phys. Lett. **39**, 397 (1981).
[3] C. Daboo, R. J. Hicken, E. Gu, M. Gester, S. J. Gray, D. E. P. Eley, E. Ahmad, J. A. C. Bland, R. Ploessl, and J. N. Chapman, Phys. Rev. B **51**, 15964 (1995).
[4] G. Wastlbauer and J. A. C. Bland, Adv. Phys. **54**, 137 (2005).
[5] H.-P. Schönherr, R. Nötzel, W. Ma, and K. H. Ploog, J. Appl. Phys. **89**, 169 (2001).
[6] A. A. Veselov, A. G. Veselov, S. L. Vysotsky, A. S. Dzhumaliev, and Yu. A. Filimonov, Tech. Phys. **47**, 1067 (2002).
[7] M. Brockmann, M. Zölfl, S. Miethaner, and G. Bayreuther, J. Magn. Magn. Mater. **198&199**, 384 (1999); M. Zölfl, M. Brockmann, M. Köhler, S. Kreuzer, T. Schweinböck, S. Miethaner, F. Bensch, and G. Bayreuther, *ibid.* **175**, 16 (1997).
[8] Biao Li, J. R. Fermin, A. Azevedo, F. M. de Aguiar, and S. M. Rezende, Appl. Phys. Lett. **72**, 2760 (1998).
[9] K. G. Nath, F. Maeda, S. Suzuki, and Y. Watanabe, J. Appl. Phys. **89**, 169 (2001).
[10] J. Herfort, H.-P. Schönherr, K.-J. Friedland, and K. H. Ploog, J. Vac. Sci. Technol. B **22**, 2073 (2004).
[11] A. Ionescu, C. A. F. Vaz, T. Trypiniotis, C. M. Gürtler, H. García-Miquel, J. A. C. Bland, M. E. Vickers, R. M. Dalgliesh, S. Langridge, Y. Bugoslavsky, Y. Miyoshi, L. F. Cohen, and K. R. A. Ziebeck, Phys. Rev. B **71**, 094401 (2005); A. Ionescu, C. A. F. Vaz, T. Trypiniotis, C. M. Gürtler, M. E. Vickers, H. García-Miquel, and J. A. C. Bland, J. Magn. Magn. Mater. **286**, 72 (2005).
[12] S. H. Liou, S. S. Malhotra, J. X. Shen, M. Hong, J. Kwo, H. S. Chen, and J. P. Mannaerts, J. Appl. Phys. **73**, 6766 (1993).
[13] J. Herfort, H.-P. Schönherr, and K. H. Ploog, Appl. Phys. Lett. **83**, 3912 (2003).
[14] Y. Nakamura, *Landolt-Börnstein, New Series III/19c* (Springer, Berlin, 1988), p. 26.
[15] A. Kawaharazuka, M. Ramsteiner, J. Herfort, H.-P. Schönherr, H. Kostial, and K. H. Ploog, Appl. Phys. Lett. **85**, 3492 (2004).
[16] J. Smit and H.-G. Beljers, Philips Res. Rep. **10**, 113 (1955).
[17] M. Farle, Rep. Prog. Phys. **61**, 755 (1998).
[18] M. Madami, S. Tacchi, G. Carlotti, G. Gubbiotti, and R. L. Stamps, Phys. Rev. B **69**, 144408 (2004).
[19] M. Goto and T. Kamimori, J. Phys. Soc. Jpn. **52**, 3710 (1983).
[20] B. Jenichen, V. M. Kaganer, J. Herfort, D. K. Satapathy, H. P. Schönherr, W. Braun, and K. H. Ploog, Phys. Rev. B **72**, 075329 (2005).
[21] J. W. Freeland, I. Coulthard, W. J. Antel, Jr., and A. P. J. Stampfl, Phys. Rev. B **63**, 193301 (2001).
[22] R. Moosbühler, F. Bensch, M. Dumm, and G. Bayreuther, J. Appl. Phys. **91**, 8757 (2002).
[23] O. Thomas, Q. Shen, P. Schieffer, N. Tournerie, and B. Lépine, Phys. Rev. Lett. **90**, 017205 (2003).
[24] G. A. Prinz, *Ultrathin Magnetic Structures II*, edited by B. Heinrich and J. A. C. Bland (Springer-Verlag, Berlin, 1994).